Covarying Alterations in Aβ Deposition, Glucose Metabolism, and Gray Matter Volume in Cognitively Normal Elderly

Hwamee Oh,[1]* Christian Habeck,[2] Cindee Madison,[1] and William Jagust[1,3]

[1]*Helen Wills Neuroscience Institute, University of California-Berkeley, Berkeley, California*
[2]*Taub Institute, Columbia University Medical School, New York, New York*
[3]*Life Sciences Division, Lawrence Berkeley National Laboratory, Berkeley, California*

Abstract: β-Amyloid (Aβ), a feature of Alzheimer's disease (AD) pathology, may precede reduced glucose metabolism and gray matter (GM) volume and cognitive decline in patients with AD. Accumulation of Aβ, however, has been also reported in cognitively intact older people, although it remains unresolved whether and how Aβ deposition, glucose metabolism, and GM volume relate to one another in cognitively normal elderly. Fifty-two cognitively normal older adults underwent Pittsburgh Compound B–positron emission tomography (PIB-PET), [^{18}F]fluorodeoxyglucose-PET, and structural magnetic resonance imaging to measure whole-brain amyloid deposition, glucose metabolism, and GM volume, respectively. Covariance patterns of these measures in association with global amyloid burden measured by PIB index were extracted using principal component analysis–based multivariate methods. Higher global amyloid burden was associated with relative increases of amyloid deposition and glucose metabolism and relative decreases of GM volume in brain regions collectively known as the default mode network including the posterior cingulate/precuneus, lateral parietal cortices, and medial frontal cortex. Relative increases of amyloid deposition and glucose metabolism were also noted in the lateral prefrontal cortices, and relative decreases of GM volume were pronounced in hippocampus. The degree of expression of the topographical patterns of the PIB data was further associated with visual memory performance when controlling for age, sex, and education. The present findings suggest that cognitively normal older adults with greater amyloid deposition are relatively hypermetabolic in frontal and parietal brain regions while undergoing GM volume loss in overlapping brain regions. *Hum Brain Mapp 00:000–000, 2012.*

Key words: β-amyloid; PET; glucose metabolism; gray matter volume; aging

INTRODUCTION

Neuritic β-amyloid (Aβ) plaques are a prominent biomarker of Alzheimer's disease (AD) pathology [Braak and Braak, 1991]. Events associated with Aβ deposition appear to include reduced glucose metabolism and brain atrophy, ultimately leading to dementia [Hardy and Selkoe, 2002; Jack et al., 2010]. Aβ deposition can be imaged in humans using amyloid-binding ligands such as Pittsburgh Compound B (PIB) and positron emission tomography (PET). PIB-PET studies reported increased Aβ deposition in the frontal cortex, temporal cortices, parietal cortices, posterior

Contract grant sponsor: NIH; Contract grant numbers: R01-AG034570, 5R01-AG026114; Contract grant sponsors: Alzheimer's Association.

*Correspondence to: Hwamee Oh, University of California-Berkeley, 132 Barker Hall, MC #3190, Berkeley, CA 94720-3190.
E-mail: hwameeoh@berkeley.edu

Received for publication 11 April 2012; Revised 30 June 2012; Accepted 13 July 2012

DOI: 10.1002/hbm.22173
Published online in Wiley Online Library (wileyonlinelibrary.com).

cingulate, and precuneus in patients with AD compared with healthy elderly individuals [Buckner et al., 2005; Buckner et al., 2009; Jack et al., 2008]. Studies examining other biomarkers in patients with AD and mild cognitive impairment (MCI) have further indicated that brain regions collectively known as the default mode network (DMN), including highly interconnected cortical hubs [Buckner et al., 2009], undergo reduced functional connectivity [Sorg et al., 2007], brain atrophy [Buckner et al., 2005; Dickerson et al., 2009], disrupted deactivation [Sperling et al., 2009], and hypometabolism [Chetelat et al., 2008; Minoshima et al., 1997].

Accumulation of Aβ has also been reported in ~20–30% of cognitively intact older people, although it remains unclear whether and how Aβ deposition and other biological measures relate to one another prior to the appearance of clinical symptoms. Animal studies have shown that accumulation of Aβ is region specific and relates to steady-state concentration of interstitial fluid (ISF) Aβ in brain regions early in life before plaque accumulation [Bero et al., 2011; Yan et al., 2009] and that the amount of ISF Aβ is associated with regional neuronal activity [Bero et al., 2011]. In humans, some studies have shown that region-specific Aβ accumulation spatially overlaps with brain regions showing aerobic glycolysis or higher functional magnetic resonance imaging (fMRI) signals indicating a positive relationship between amyloid deposition and metabolism [Vaishnavi et al., 2010; Vlassenko et al., 2010] or brain activity [Sperling et al., 2009]. Other studies, however, show the relationship between amyloid deposition and glucose metabolism to be the same in normal aging and AD [Drzezga et al., 2011]. In addition, Aβ and brain atrophy are related in patients with AD and MCI [Buckner et al., 2005; Tosun et al., 2011] and cognitively normal elderly [Becker et al., 2011; Bourgeat et al., 2010; Mormino et al., 2009; Oh et al., 2011], but the degree of the overlapping topographic distribution between amyloid deposition and brain atrophy in aging is unclear.

To examine the regional patterns of Aβ deposition, glucose metabolism, and gray matter (GM) volume and their relationship with cognitive performance in aging, we applied a principal component analysis–based multivariate method, Scaled Subprofile Model (SSMPCA), to the analysis of [^{18}F]fluorodeoxyglucose (FDG)-PET, PIB-PET, and structural MRI data [Alexander and Moeller, 1994; Habeck et al., 2008]. Specific aims were twofold. One was to examine whether and how topographical patterns of Aβ deposition, glucose metabolism, and GM volume relate to one another in cognitively normal elderly. The other was to examine whether the pattern of amyloid deposition or associated structural and functional change is associated with cognition.

METHODS

Participants

Fifty-two healthy older adults [mean age = 74.1 ± 6.0 years, 34 females, mean Mini-Mental State Examination (MMSE) = 29.1 ± 1.1] participated in the study (Table I). All subjects were a subgroup of individuals who were recruited from the community via newspaper advertisements and completed PIB-PET, FDG-PET, and structural MRI scans. All subjects underwent a medical interview and a detailed battery of neuropsychological tests. In order to be eligible for the study, subjects were required to be 60 years or older, live independently in the community without neurological or psychiatric illness, and have no major medical illness or medication that influence cognition. To generate cognitive composite scores from neuropsychological tests, we used scores from a total of 254 cognitively intact older adults (mean age: 74.0 ± 7.4 years, range: 60–96 years, 167 females, mean MMSE = 28.6 ± 1.6) who underwent cognitive testing but did not undergo neuroimaging. All subjects provided informed consent in accordance with the Institutional Review Boards of the University of California, Berkeley and the Lawrence Berkeley National Laboratory (LBNL) prior to their participation.

TABLE I. Characteristics of subjects

N	52
Age (years)	74.11 (6.02)[a]
Education (years)	17.21 (1.94)
Gender (*n*, F/M)	34/18
PIB index	1.12 (0.20)
APOE-ε4 (*n* [%])[b]	16 (31%)
TIV	1586.6 (163.16)
MMSE	29.08 (1.07)

TIV, total intracranial volume; PIB, Pittsburgh compound B; MMSE, Mini-Mental State Examination.
[a]Mean and standard deviation in parentheses.
[b]Proportion of individuals with APOE genotypes ε3/4 or ε4/4.

Neuropsychological Cognitive Measures

All subjects underwent a detailed battery of neuropsychological tests that encompass multiple cognitive domains. The tests included Free Recall Trials 1–5, Short-Delay Free Recall, Short-Delay Cued Recall, Long-Delay Free Recall, and Long-Delay Cued Recall of California Verbal Learning Test (CVLT) II [Delis et al., 2000], Stroop Test [Golden, 1978], "Trail B" and "Trail B minus A" scores from Trail Making Test A and B [Reitan, 1958], Symbol Digit Modalities Test [Smith, 1982], category "Vegetables" and "Animals" from Category Fluency Test [Benton et al., 1983], Digit span forward and backward, Immediate Recall (VRI Recall Total), Delayed Recall (VRII Recall Total), Retention (VR % Retention) and Recognition (VR Recognition Total) from the Visual Reproduction (VR) Test in the Wechsler Memory Scale-Third Edition (WMS-III) [Wechsler, 1997], and Recall of Story A and Story B from Logical Memory [WMS-III; Wechsler, 1997]. To generate a composite score from neuropsychological tests, all

test scores from subjects in the subject pool were entered into an exploratory factor analysis with varimax rotation. Among factors extracted by the method, five factors that maximize the sum of variance explained were selected for this study and, based on the type of individual tests that express the highest factor loading scores for the factor, each factor was named as follows: executive function (EXE), episodic memory (EM), semantic memory (SM), working memory (WM), and visual memory (VM). Subjects' factor scores were entered in subsequent multiple regressions to examine the relationship with the degree of pattern expressions as quantified by subject scaling factors (SSFs) in SSMPCA for Aβ deposition (SSF-PIB), glucose metabolism (SSF-FDG), and GM volume (SSF-VBM), respectively.

Imaging Data Acquisition

PIB-PET

[*N*-methyl-^{11}C]-2-(4′-methylaminophenyl)-6-hydroxybenzothiazole ([^{11}C]PIB) was synthesized at LBNL's Biomedical Isotope Facility using a previously published protocol [Mathis et al., 2003]. All PET scans were performed at LBNL using a Siemens ECAT EXACT HR PET scanner in three-dimensional acquisition mode. Dynamic acquisition frames (total of 34 frames) were obtained over 90 min as follows: 4 × 15 s, 8 × 30 s, 9 × 60 s, 2 × 180 s, 8 × 300 s, and 3 × 600 s. Approximately 15 mCi of [^{11}C]PIB was injected as a bolus into an antecubital vein.

FDG-PET

[^{18}F] FDG was purchased from a commercial vendor (IBA Molecular, Morgan Hill, CA). At a minimum of 2 h following ^{11}C-PIB injection, subjects were injected with 6–10 mCi of [^{18}F] FDG. Six emission frames of 5 min each were acquired starting 30 min after tracer injection, with the subject resting quietly in a dimly lit room with eyes and ears unoccluded during tracer uptake.

For both PIB-PET and FDG-PET, 10-min transmission scans for attenuation correction were obtained either immediately prior to or following each ^{11}C-PIB and ^{18}F-FDG scan. PET data were reconstructed using an ordered subset expectation maximization algorithm with weighted attenuation. Images were smoothed with a 4-mm Gaussian kernel with scatter correction.

Structural MRI

High-resolution structural MRI scans were collected at LBNL on a 1.5-T Magnetom Avanto system (Siemens, Iselin, NJ) with a 12-channel head coil run in triple mode. Three high-resolution T_1-weighted magnetization-prepared rapid gradient echo scans were collected axially for each subject (repetition time (TR) = 2,110 ms, echo time (TE) = 3.58 ms, flip angle: 15°, field of view = 256 × 256 mm^2, matrix size: 256 × 256 mm^2, slices: 160, and voxel size = 1 × 1 × 1 mm^3).

Imaging Data Analysis

All PET images were preprocessed using Statistical Parametric Mapping 8 (SPM8; http://www.fil.ion.ucl.ac.uk/spm/). Region of interest (ROI) labeling was implemented using the FreeSurfer v4.4 software package (http://surfer.nmr.mgh.harvard.edu/) to create reference regions in the GM cerebellum and pons and to perform subsequent ROI analyses.

PIB-PET

The first five PIB frames were summed and all PIB frames including the summed image from one to five frames were realigned to the middle (17th) frame. The subject's structural MRI image was coregistered to realigned PIB frames. PIB distribution volume ratio (DVR) was calculated on a voxel-wise level using Logan graphical analysis and the subject's GM cerebellar reference region with frames corresponding to 35–90 min postinjection [Logan et al., 1996; Price et al., 2005]. DVR images warped to the Montreal Neurological Institute (MNI) template were smoothed with an 8-mm full-width at half-maximum (FWHM) Gaussian kernel.

FDG-PET

Six frames of FDG-PET were realigned using the first frame as a reference and a mean FDG image was generated. The FDG PET mean image was coregistered to the mean PIB PET image, followed by coregistration of the subject's structural MRI image (and associated MRI-defined reference regions) to the mean FDG image. This resulted in having FDG and PIB images in the same space for subsequent analysis. The realigned FDG frames were summed across frames and the summed image was intensity normalized on a voxel-wise level to the mean value of the pons. Pons-normalized FDG images were warped to an Montreal Neurological Institute (MNI) structural template via the subject's MRI and smoothed with an 8-mm FWHM Gaussian kernel.

Structural MRI

We performed VBM implemented with SPM8 running under Matlab 7.7 (Mathworks, Natick, MA) on structural images. VBM is a semiautomated iterative procedure in which implementations of tissue classification, bias correction, and nonlinear warping are combined. Details can be found in the previously published report [Oh et al., 2011]. Briefly, the VBM procedure implemented in this study included segmentation, normalization, modulation, and smoothing steps. First, an averaged single structural T_1 image for each subject was segmented into GM, white

matter (WM), and cerebral spinal fluid (CSF) using GM, WM, and CSF tissue probability maps provided by SPM8. Segmented GM and WM were then spatially normalized to the International Consortium for Brain Mapping GM and WM templates using the 12-parameter affine transformation [Ashburner et al., 1997] and nonlinear registration [Ashburner and Friston, 1999]. Warped images were then modulated by the Jacobian determinants derived from the spatial normalization step in order to adjust for the resulting volume changes due to warping [Good et al., 2001]. Modulated warped images were smoothed with a 12-mm Gaussian kernel at the FWHM. Total intracranial volume (TIV) was calculated by summing volumes of GM, WM, and CSF derived from segmented images in native space.

ROIs for a Global PIB Index

For all subjects, an averaged single structural T_1 image was processed through Freesurfer v4.4 to implement ROI labeling. Details can be found in the previously published report [Oh et al., 2011]. Briefly, structural images were bias field corrected, intensity normalized, and skull stripped using a watershed algorithm, followed by a WM-based segmentation, defining GM/WM and pial surfaces, and topology correction [Dale et al., 1999; Fischl et al., 2001; Segonne et al., 2004]. Subcortical and cortical ROIs spanning the entire brain were defined in each subject's native space [Desikan et al., 2006; Fischl et al., 2002]. The resulting cerebellum ROI (GM only) was used as a reference region to create a PIB-DVR image. The resulting brainstem ROI by the Freesurfer processing stream was manually edited to generate a pons ROI that was used to normalize FDG data for each individual. Large cortical ROIs spanning frontal, temporal, and parietal cortices, and anterior/posterior cingulate gyri were constructed as previously described [Oh et al., 2011]. Mean DVR values from these large ROIs constituted a global PIB index for each subject.

Scaled Subprofile Modeling Analysis

To extract covarying patterns in PIB, FDG, and VBM data that are associated with PIB index of each subject, we applied Scaled Subprofile Modeling (SSM) analysis to the preprocessed PIB, FDG, and VBM data using SPM 5 on Matlab version 7.4 (Math Works, Natick, MA). As a modified form of PCA, SSM identifies spatial covariance patterns that are associated with a variable of interest (i.e., PIB index in this study) on a voxel basis across the whole brain. The assumptions and procedures of the SSM have been described in detail in previous studies [Alexander and Moeller, 1994; Alexander et al., 2008; Habeck and Stern, 2010; Moeller et al., 1987]. Briefly, prior to principal component (PC) extraction, the GM mask with a threshold >0.4 was applied to the PIB-PET, FDG-PET, and VBM data to include voxels that are most likely GM. This procedure assures that the same GM map was used throughout three imaging modalities. Then, we subtracted group mean voxel values across regions and participants from the raw values at each voxel for each participant for each modality. This step effectively normalizes each voxel for total brain measures and subject mean differences before the PCA. Thus, SSM extracts the variance reflecting the region by subject interaction in the imaging data after removing the main effects for global brain measures and subject differences on a voxel basis [Alexander et al., 2006]. For the PIB-PET and FDG-PET data, brain volume ratio that was calculated by the sum of GM and WM divided by the TIV was entered as a nuisance covariate in the regression analyses to account for effects of brain atrophy. These regression models were applied to select a combination of PCs in association with PIB index. TIV was entered as a nuisance covariate in the regression analysis for the VBM data to eliminate the main effect of head size.

We performed separate SSMPCAs on PIB-PET, FDG-PET, and VBM data to identify patterns of Aβ deposition, glucose metabolism, and GM volume related to global PIB index characterizing overall Aβ deposition across the whole brain regions in cognitively intact normal elderly. Akaike Information Criteria (AIC) were applied to identify the best set of SSM component patterns predicting a global PIB index [Akaike, 1973]. After applying AIC to determine the PCs to be included, nonparametric regression with 10,000 permutations (i.e., permutation tests in the text below) were implemented to test the hypothesis of a significant relationship between PIB index and covariance patterns of PIB-PET, FDG-PET, and VBM data. The relationship was evaluated at $P < 0.05$. In addition, a bootstrap resampling procedure was implemented to estimate the variability of the regional weights in the patterns about their point estimate values with a 500 iteration resampling procedure with replacement [Habeck et al., 2005]. A Z-value threshold $\geq |1|$ for FDG-PET and VBM data and a Z-value threshold $\geq |3|$ for PIB-PET data were adopted purely for visualization purposes to show the full extent of brain regions contributing to the combined SSM pattern. It is important to note that bootstrapping was conducted to estimate voxel-wise variability, which is analogous to univariate approaches, and the resulting statistics are not for hypothesis testing unlike the permutation tests that were adopted to test hypotheses about the association between PIB index and covariance patterns.

Multiple Regressions With Cognitive Test Scores

All nonimage analyses were conducted using SPSS software (version 19). Multiple regressions were used to assess the relationship between the degree of pattern expression as quantified by the SSFs and cognitive performance. That is, we conducted multiple regressions for a total of three pattern expression scores (i.e., SSF-PIB, SSF-FDG, and SSF-VBM) and five cognitive factor scores (i.e., EM, VM, EXE, SM, and WM) with each SSF score being a predictor of

interest and each cognitive factor score being a dependent measure, resulting in 15 regression models. Age, sex, and education were controlled in all analyses. Statistical significance was determined at $P < 0.05$.

RESULTS

Characteristics of Subjects

Subject characteristics are summarized in Table I. Factor analysis on neuropsychological measures revealed five components (i.e., EXE, EM, SM, WM, and VM) that accounted for 77.1% of the total variance of the data. Higher factor loadings were weighted on CVLT subtests and Logical Memory for EM; visual reproduction subtests for VM; category fluency subtests for SM; digit span subtests for WM; and Trail Making subtests and Stroop for EXE. Because of the nature of factor analysis, however, all neuropsychological test scores contributed to each factor score to a varying degree.

The Aβ Topography Associated With a Global PIB Index

The association between the global PIB index and Aβ deposition topography was tested by a multiple regression model with SSM subject factor scores for the eight component patterns selected by AIC. The linear combination of the selected eight PCs (i.e., PCs 1, 2, 3, 4, 5, 6, 8, and 10) accounted for 98% of the variance in the PIB data (i.e., $R^2 = 0.98$), and the permutation test showed that the patterns of a linear combination of PCs significantly predicted the PIB index, $P < 0.001$. The identified covariance pattern of the PIB data in association with a global PIB index is presented in Figure 1A, and the relation between SSF-PIB and PIB index is shown in Figure 2A. Peak coordinates of suprathreshold clusters are listed in Table II. As shown in Figure 1A and Table II, relatively reduced amyloid deposition indicated by voxels with negative loadings, corresponding to PIB-related decreases in values, was identified in the hippocampus bilaterally and visual and motor cortex. Regions with positive loadings, indicating PIB-related increases in values, were observed in the medial frontal cortex, temporoparietal cortex, lateral parietal cortex, and precuneus. In Figure 2A, greater expression of the covariance pattern of the PIB data as evidenced by higher SSF scores was significantly associated with higher overall PIB deposition.

The FDG Topography Associated With a Global PIB Index

A linear combination of two component patterns (i.e., PCs 3 and 12) selected by AIC significantly predicted PIB index, $R^2 = 0.15$, $P < 0.05$. Figure 1B shows the FDG pattern in association with the PIB index, and Figure 2B illustrates the significant association between PIB index and SSF-FDG. The pattern for glucose metabolism associated with increased Aβ deposition was characterized by relative decreases in the inferior medial frontal cortex, lateral and medial temporal cortex, anterior cingulate, and visual cortex and relative increases in the lateral prefrontal cortex, lateral parietal cortex, and precuneus. Table III lists peak coordinates of suprathreshold clusters.

The GM Volume Topography Associated With a Global PIB Index

Figure 1C shows the topographic pattern of GM volume in relation to the PIB index, and Table IV shows the list of peak coordinates of suprathreshold clusters. The association between component (i.e., PC 4) pattern scores and the PIB index showed a trend toward significance, $R^2 = 0.04$, $P = 0.10$ (Fig. 2C). A topographic pattern of GM volume in association with the PIB index was characterized by negative loadings in the medial frontal, lateral temporal, and posterior cingulate cortices and hippocampus and positive loadings in the superior frontal, primary sensory/motor, and visual cortices as illustrated in Figure 1C.

Associations of Amyloid Deposition, Glucose Metabolism, and MRI GM Volume Covariance Patterns With Cognition

We evaluated the association between SSF scores and cognitive performance measured by factor scores using multiple regressions. Multiple regressions showed a significant association between SSF-PIB and visual memory, $\beta = -0.30$, $P < 0.05$, indicating that a greater expression of the amyloid deposition pattern is related to worse visual memory. No association was found for either SSF-FDG or SSF-VBM and any other cognitive measures. The relationship between SSF-PIB scores and visual memory is illustrated in Figure 3.

DISCUSSION

In this study, we examined covariance patterns of Aβ deposition, glucose metabolism, and GM volume that are associated with Aβ to elucidate the topographical relationships between these processes in cognitively normal older adults. Covariance patterns for each modality in relation to a global PIB index strikingly corresponded with each other in their spatial extent. The directionality between Aβ deposition, glucose metabolism, and GM volume, however, was different from that reported in patients with clinical symptoms of AD. Unlike patients with AD who show hypometabolism along with higher Aβ deposition in brain regions that are considered to be vulnerable to AD pathology, cognitively intact older adults with higher levels of Aβ deposition showed relative increases of both glucose metabolism and Aβ deposition in overlapping brain regions, the posterior cingulate/precuneus, and lateral

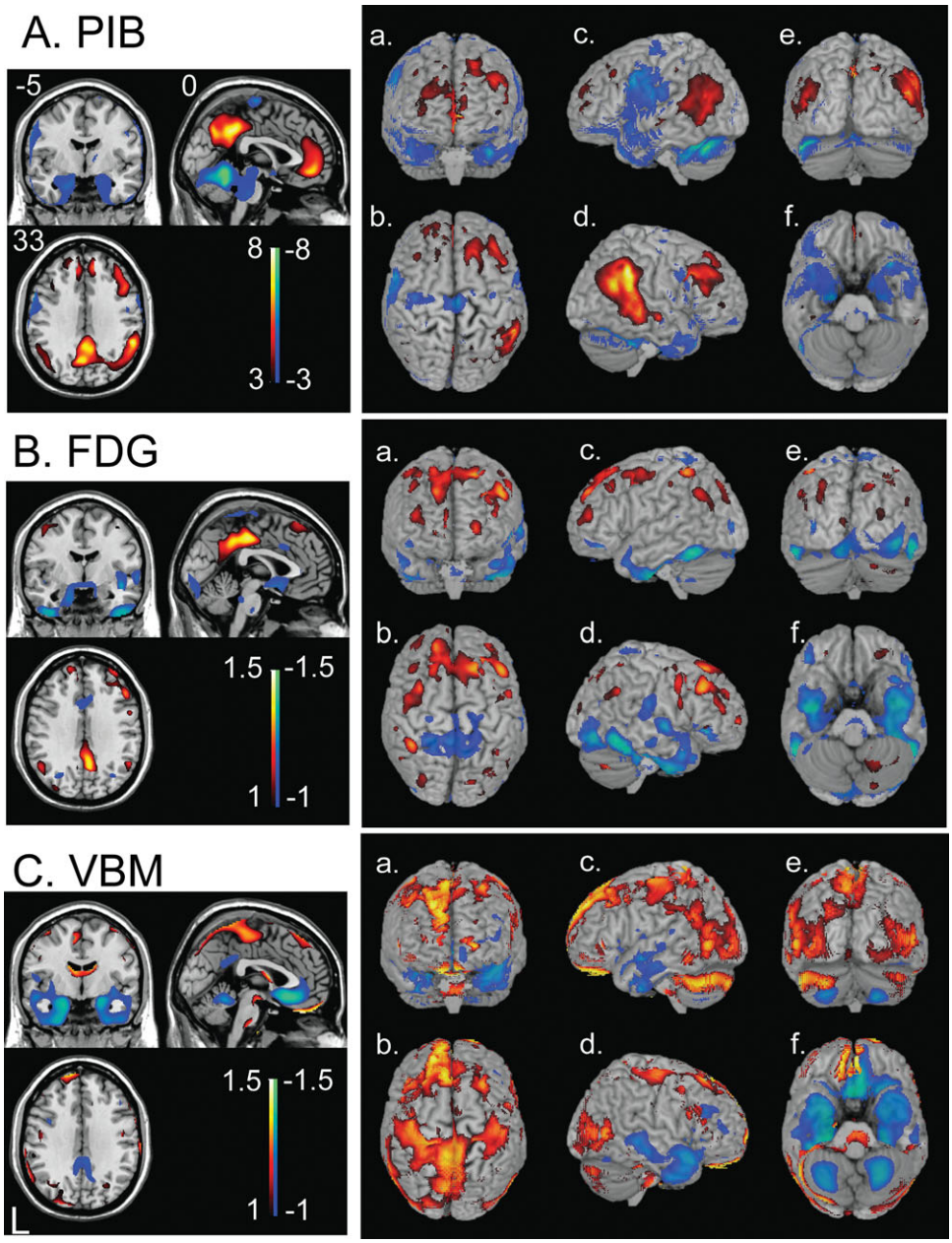

Figure 1.

PIB, FDG, and VBM covariance patterns reflecting the linear combination of SSM components in association with a global measure of amyloid deposition. Covariance patterns of amyloid deposition (**A**), glucose metabolism (**B**), and gray matter volume (**C**) reflecting a linear combination of SSM components that best explains the global PIB index. Voxels with positive loadings (warm colors) and negative loadings (cool colors) in association with global PIB index for PIB (A), FDG (B), and VBM (C) data are superimposed in coronal, sagittal, and axial slices in MNI space ($X = -5$, $Y = 0$, and $Z = 33$) shown in the left panels. In addition, these voxels are projected onto the anterior and posterior surfaces (a and e), the left and right lateral surfaces (c and d), and the dorsal and ventral surfaces (b and f) of the rendered MNI single-subject brain. Voxels with positive loadings indicate greater amyloid deposition, glucose metabolism, and gray matter volume with higher global PIB index. Voxels with negative loadings indicate lower amyloid deposition, glucose metabolism, and gray matter volume with increased global PIB index. Voxels with *Z*-scores $\geq|1|$ for FDG and VBM data and voxels with *Z*-scores $\geq|3|$ for PIB data after bootstrap resampling are shown for visualization of regional patterns. Cluster threshold: 50 voxels. L, left. [Color figure can be viewed in the online issue, which is available at wileyonlinelibrary.com.]

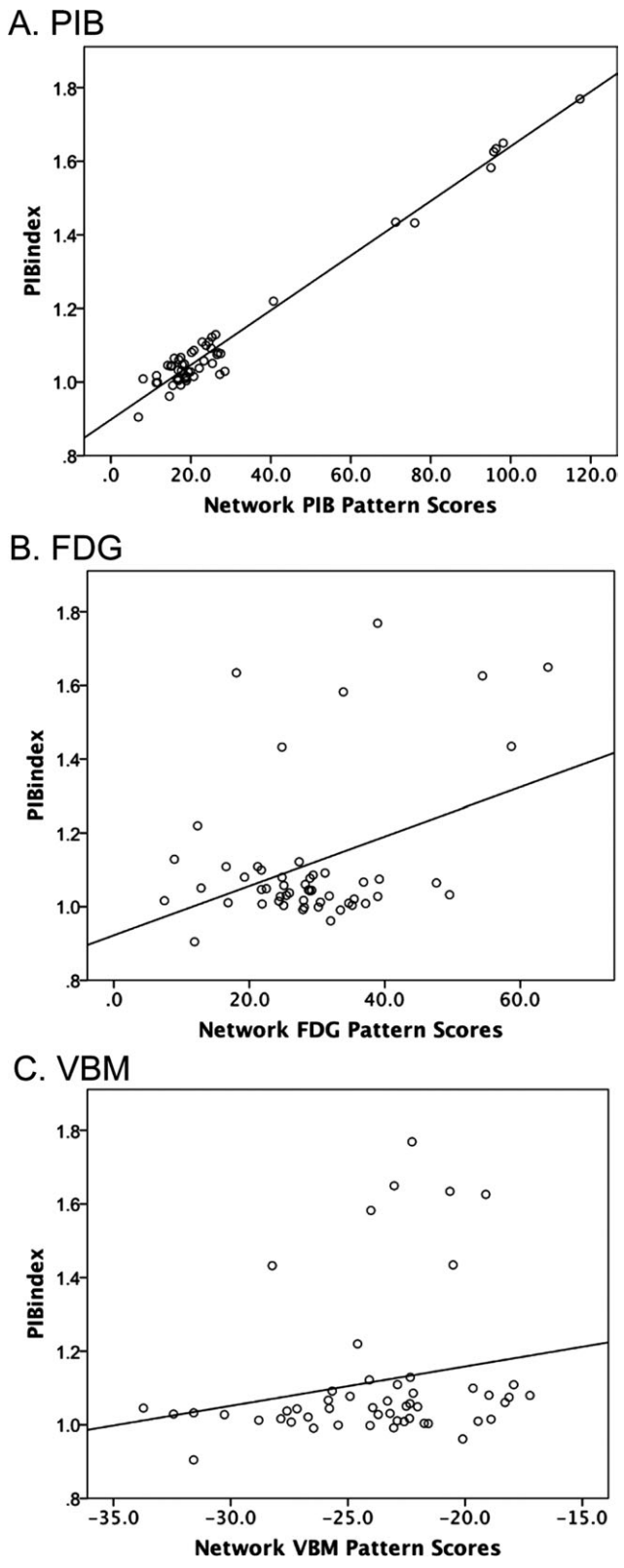

parietal and prefrontal cortices in particular. GM volume changes in relation to Aβ deposition, however, were consistent with previous findings showing greater GM volume reduction in brain regions susceptible to AD pathology.

Relationships of Aβ Deposition, Glucose Metabolism, and GM Volume in Patients With AD and MCI

Hypometabolism and Aβ deposition have been considered as pathological characteristics of AD and MCI [Minoshima et al., 1997; Silverman et al., 2001], particularly in brain regions involving the DMN [Buckner et al., 2005; Edison et al., 2007; Klunk et al., 2004]. The PIB pattern identified by SSMPCA in this study reflects what other studies have shown about the regional deposition of Aβ, by displaying increased PIB binding in the precuneus, lateral parietal cortices, and medial and lateral frontal cortices. Regional topography of atrophy in this study is also consistent with previous cross-sectional and longitudinal studies that have indicated prominent brain atrophy in AD particularly in the medial temporal lobe, the lateral temporoparietal cortex, and basal temporal lobe [Jack et al., 2008, 2009]. Some brain regions, notably inferomedial temporal cortex, also showed atrophy and hypometabolism in the absence of Aβ deposition. The present findings of topographical patterns of amyloid deposition and GM volume reduction in association with global PIB index indicate that brain regions known to be susceptible to AD pathology undergo both increased amyloid deposition and GM reduction in normal aging, while some regions express hypometabolism as well.

Relationships of Aβ Deposition, Glucose Metabolism, and GM Volume in Cognitively Normal Elderly

Aβ deposition clearly occurs in older people without clinical symptoms [Aizenstein et al., 2008; Bennett et al.,

Figure 2.

Association between PIB index and subject scaling scores resulting from the linear combination of the SSM components for PIB, FDG, and VBM measures. A regression scatterplot illustrating the relationship of global PIB index and covariance pattern scores (i.e., SSF scores) in PIB (**A**), FDG (**B**), and VBM (**C**) data. The *x*-axis of each scatterplot represents covariance pattern scores for PIB (SSF-PIB), FDG (SSF-FDG), and VBM (SSF-VBM) data, respectively. The *y*-axis represents a global PIB index. The relationships assessed by nonparametric regression were statistically significant between global PIB index and SSF-PIB ($R^2 = 0.98$, $P < 0.05$) and between global PIB index and SSF-FDG ($R^2 = 0.15$, $P < 0.05$). The relationship between global PIB index and SSF-VBM was marginally significant ($R^2 = 0.04$, $P = 0.10$).

TABLE II. SSMPCA clusters and peak coordinates in the PIB covariance pattern in association with global PIB index

Cluster size	X	Y	Z	Z Statistics	Regions
Positive loadings					
9,263	8	−38	44	8.72	R middle cingulate
	0	−48	36	7.53	Precuneus
5,781	6	50	−2	8.54	R mid orbital
2,264	−48	−62	16	5.27	L middle temporal
228	−56	−18	−8	4.19	L middle temporal
83	−42	−36	−18	4.04	L inferior temporal
168	−36	26	42	4.02	L middle frontal
Negative loadings					
14,703	2	−56	−12	−8.46	Cerebellar vermis
2,813	34	20	−36	−6.46	R med temporal pole
	18	0	−26	−5.35	R parahippocampal
352	2	−18	72	−5.80	R suppl. motor area
214	−40	−14	66	−5.01	L precentral
81	32	58	−16	−4.08	R middle orbital
65	54	−64	−36	−4.05	R cerebellum

TABLE III. SSMPCA clusters and peak coordinates in the FDG covariance pattern in association with global PIB index

Cluster size	X	Y	Z	Z Statistics	Regions
Positive loadings					
3,415	8	−32	52	1.49	R paracentral lobule
	0	−26	42	1.42	Posterior cingulate
	6	−54	35	1.41	R precuneus
2,200	20	28	54	1.33	R superior frontal
852	46	28	36	1.32	R middle frontal
164	−42	−46	56	1.3	L inferior parietal
978	38	−64	−40	1.27	R cerebellum
656	−34	10	52	1.25	L middle frontal
239	−44	−42	−14	1.22	L inferior temporal
405	38	16	10	1.22	R inferior frontal
258	52	4	40	1.19	R precentral
260	−50	−58	36	1.18	L angular
Negative loadings					
374	−56	−54	−20	−1.41	L inferior temporal
4,194	56	−48	−22	−1.4	R inferior temporal
3,104	−40	−10	−44	−1.39	L inferior temporal
1,725	42	−78	−12	−1.34	R inferior occipital
131	54	30	−6	−1.32	R inferior frontal
74	−38	−38	38	−1.28	L inferior parietal
84	−46	40	−16	−1.22	L inferior frontal
1,095	−20	−42	70	−1.2	L postcentral
73	−30	−68	30	−1.2	L middle occipital
83	−44	−10	−8	−1.18	L superior temporal
357	−4	12	36	−1.15	L anterior cingulate
115	−46	−36	6	−1.13	L superior temporal
112	−4	−20	−38	−1.13	Pons

2006]. Compared to the findings in patients with AD, however, the relationship between Aβ deposition and other AD-related biomarkers is not as clear in cognitively normal older adults. For example, the apolipoprotein E4 allele is associated with increased risk of AD, glucose hypometabolism in typically vulnerable regions in asymptomatic people [Reiman et al., 2004], and subsequent memory decline [Caselli et al., 2004]. Although this suggests that metabolic changes in cognitively normal people with AD vulnerability may parallel those seen in AD subjects, Cohen et al. [2009] have shown that glucose metabolism is higher with greater Aβ in these same brain regions in patients with MCI. Therefore, although limited, emerging literature seems to suggest a possible positive relationship between metabolism and Aβ accumulation in brain regions that are known to be susceptible to AD pathology before severe clinical AD symptoms appear.

Hypometabolism in relation to Aβ accumulation has been widely interpreted as evidence of disrupted neuronal functions and synaptic activity. Causes of relatively increased glucose metabolism in relation to higher level of Aβ accumulation, however, are not clear. One possible explanation may be activated microglia found within and immediately surrounding maturing amyloid plaques [Itagaki et al., 1989]. Aβ-related microgliosis, astrocytosis, and the overproduction and release of various inflammatory mediators may explain the increased level of glucose metabolism [Fellin et al., 2004; Palop and Mucke, 2010; Vezzani and Granata, 2005]. Another possibility is an increase of the abnormally hyperactive neurons in cortical circuits [Abramov et al., 2009; Busche et al., 2008; Palop and Mucke, 2009; Puzzo et al., 2008; Vezzani and Granata, 2005]. Another possible mechanism may be altered ionic homeostasis, particularly excessive calcium entry into neurons and increases in astroglial calcium ions [Selkoe, 2001].

TABLE IV. SSMPCA clusters and peak coordinates in the VBM covariance pattern in association with global PIB index

Cluster size	X	Y	Z	Z Statistics	Regions
Positive loadings					
605	0	36	−32	1.49	R rectal
	−8	32	−30	1.45	L rectal
15,432	−18	54	38	1.44	L superior frontal
228	18	70	−4	1.42	R middle orbital
852	12	−2	20	1.38	R caudate
669	−54	−64	−38	1.37	L cerebellum
80	56	−34	−30	1.37	R inferior temporal
974	22	−94	−18	1.36	R lingual temporal
191	32	−88	−32	1.21	R cerebellum
127	66	−36	40	1.23	R supramarginal
99	16	−78	14	1.18	R calcarine
97	42	8	22	1.25	R inferior frontal
Negative loadings					
23,232	8	10	−12	−1.46	R caudate
738	24	−64	−52	−1.31	R cerebellum
665	−28	−72	−50	−1.28	L cerebellum
144	46	28	24	−1.2	R inferior frontal
97	40	48	6	−1.14	R middle frontal

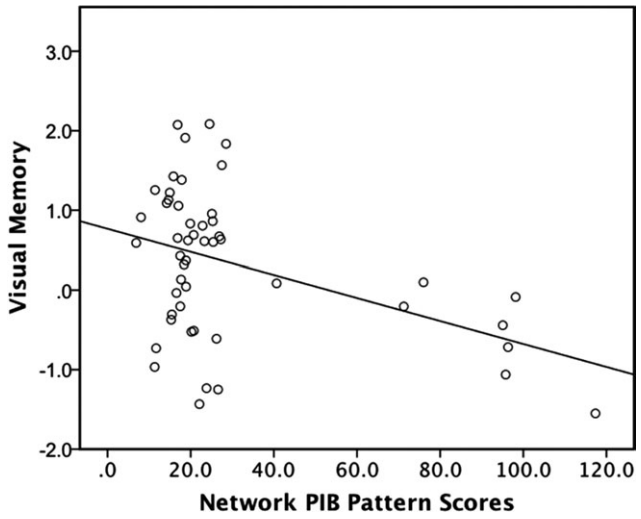

Figure 3.

Association between visual memory performance and PIB subject scaling scores. A scatterplot illustrating the relationship of covariance pattern scores of PIB data (SSF-PIB) and visual memory component scores. The *x*-axis of the scatterplot represents covariance pattern scores of PIB data and the *y*-axis represents visual memory component scores. The relationship between SSF-PIB and visual memory was statistically significant, $\beta = -0.30$, $P < 0.05$, when age, sex, and education were controlled for.

All these possibilities are considered as metabolic consequences of increased accumulation of Aβ.

Functional associations may also explain the associations between Aβ deposition and higher metabolism, indirect measures of increased neural activity that leads to overproduction of Aβ. Direct evidence of the causal relation between neural activity and production of Aβ has been provided in animal studies [Bero et al., 2011; Cirrito et al., 2005; Kamenetz et al., 2003; Kang et al., 2009]. The associations between higher metabolism and Aβ deposition seen in patients with MCI [Cohen et al., 2009] are also consistent with a view that higher basal metabolism may lead to acceleration of amyloid deposition. Studies using fMRI have also reported increased brain activation in subjects with MCI [Dickerson et al., 2005] or PIB-positive normal controls compared with PIB-negative normal controls [Mormino et al., 2011; Sperling et al., 2009; for a review, Jagust and Mormino, 2011]. Buckner et al. [2009] also showed that brain regions accumulating greater level of amyloid as evidenced in patients with AD correspond to functional hubs identified by increased functional connectivity with other brain regions compared with the rest of the brain. The identified functional hubs include medial frontal cortex, posterior cingulate/precuneus, and lateral frontal and parietal regions and highly overlap with brain regions that show relative increase in metabolism in our results. Therefore, although metabolism, increased fMRI signal, functional connectivity, and neuronal activity may measure different aspects of brain function, a very similar topography between brain regions expressing a higher level of these functional measures and those accumulating greater amyloid deposition implicates an underlying neural mechanism that relates these phenomena. Direct causal mechanisms of increased metabolism in relation to Aβ accumulation in our results, however, cannot be resolved based on the current cross-sectional data. In addition, it is possible that increases in glucose metabolism are compensatory in nature and play a role in permitting older individuals to remain cognitively normal in the face of Aβ deposition [Kadir et al., 2012].

The regional variability seen in the covariance patterns of PIB, FDG, and VBM data raises the question of whether there is any laterality difference in these patterns. When we counted the number of voxels with negative and positive loadings for each hemisphere, there was little laterality difference, although voxels with negative loadings were slightly left-lateralized with PIB and right-lateralized with FDG covariance patterns. Because of a lack of significance testing, it is not clear whether this trend of laterality bears any significance, but future studies may examine laterality effects in regional topography of these biomarkers in relation to global amyloid deposition.

Because of the nature of the cross-sectional data in this study and the relative nature of the biological measures defined by the multivariate approach, however, it is uncertain whether the relative increases in metabolism associated with Aβ will be linked to the later development of AD. Moreover, the present results do not indicate absolute increases in glucose metabolism in association with higher amyloid deposition. The covariance analysis approach we took is designed to account for global signal in brain activity and variability in brain function among individuals that usually obscures the regional topographic patterns of interest [Alexander and Moeller, 1994]. The SSMPCA approach allowed us to examine subject–region interactions that can be clinically and/or biologically relevant but represent small effects. Therefore, the relative increases or decreases in covariance patterns identified by the multivariate analysis method are particularly useful when the effect is subtle and distributed and thereby cannot be localized to a few key regions using more traditional univariate approaches. This is relevant to the present results because pattern scores were significantly correlated with the PIB index, while voxel-based *Z*-scores of FDG and VBM covariance maps in association with the PIB index were quite low. These *Z*-maps on a voxel basis underscore the need for multivariate analysis when the effect can be captured through covariance patterns across widespread regions.

Cognitive Changes in Association With Aβ Deposition, Glucose Metabolism, and GM Volume Changes in Normal Aging

It is crucial to understand the relationship between Aβ-induced alterations at different levels of analysis: at synapses, circuits, networks, and cognition to determine what

aspect of neuronal dysfunction is most directly related to cognitive decline. The present data indicate that the pattern of Aβ accumulation is related to cognitive performance measured in visual memory, whereas neither the Aβ-dependent pattern of glucose metabolism nor that of GM volume accounts for individual differences in cognition during normal aging.

The effect of Aβ deposition, glucose metabolism, and GM volume on cognition in normal aging is not resolved. Some studies have shown no difference in GM volume and episodic memory scores between the elderly with high PIB and those with low PIB [Bourgeat et al., 2010]. Others have reported poorer cognition, episodic memory in particular, in relation to Aβ deposition during normal aging [Oh et al., 2012; Pike et al., 2007; Villemagne et al., 2008]. By correlating SSF scores, a single measure representing a degree of expression of the covariance pattern, with cognitive factor scores, we further sought to elucidate whether individual differences in cognition can be explained by the degree of expression of the patterns that were formed because of Aβ deposition. A significant association between the degree of the covariance pattern of Aβ deposition and visual memory provides support for an effect of Aβ on episodic memory, although limited to visual domains, among cognitively normal elderly. With regard to the FDG covariance patterns, there was no association between the degree of expression of the covariance pattern and cognition. This result may indicate that relatively increased metabolism in the brain regions accumulating greater Aβ reflects increased neural activity that may compensate for a deteriorating effect of Aβ on cognition. Conversely, it is also possible that some people have higher resting metabolism than others in order to perform equivalently on cognitive tests, leading to amyloid deposition. Although the current results cannot resolve this issue, future studies are warranted to directly test the temporal sequences of changes in metabolism and amyloid deposition across the lifespan.

REFERENCES

Abramov E, Dolev I, Fogel H, Ciccotosto GD, Ruff E, Slutsky I (2009): Amyloid-beta as a positive endogenous regulator of release probability at hippocampal synapses. Nat Neurosci 12:1567–1576.

Aizenstein HJ, Nebes RD, Saxton JA, Price JC, Mathis CA, Tsopelas ND, Ziolko SK, James JA, Snitz BE, Houck PR, Bi W, Cohen AD, Lopresti BJ, DeKosky ST, Halligan EM, Klunk WE (2008): Frequent amyloid deposition without significant cognitive impairment among the elderly. Arch Neurol 65:1509–1517.

Aizenstein HJ, Nebes RD, Saxton JA, Price JC, Mathis CA, Tsopelas ND, Ziolko SK, James JA, Snitz BE, Houck PR, Bi W, Cohen AD, Lopresti BJ, DeKosky ST, Halligan EM, Klunk WE. (2008). Frequent amyloid deposition without significant cognitive impairment among the elderly. Arch Neurol, 65:1509–1517.

Akaike H (1973): Information theory and an extension of the maximum likelihood principle. In: Petrov BN, Csaki F, editors. Proceedings of the Second International Symposium on Information Theory. Budapest: Akademiai Kiado. pp 267–281.

Alexander GE, Moeller JR (1994): Application of the Scaled Subprofile Model to functional imaging in neuropsychiatric disorders: A principal component approach to modeling brain function in disease. Hum Brain Mapp 2:79–94.

Alexander GE, Chen K, Merkley TL, Reiman EM, Caselli RJ, Aschenbrenner M, et al. (2006): Regional network of magnetic resonance imaging gray matter volume in healthy aging. Neuroreport 17:951–956.

Alexander GE, Chen K, Aschenbrenner M, Merkley TL, Santerre-Lemmon LE, Shamy JL, et al. (2008): Age-related regional network of magnetic resonance imaging gray matter in the rhesus macaque. J Neurosci 28:2710–2718.

Ashburner J, Friston KJ (1999): Nonlinear spatial normalization using basis functions. Hum Brain Mapp 7:254–266.

Ashburner J, Neelin P, Collins DL, Evans A, Friston K (1997): Incorporating prior knowledge into image registration. Neuroimage 6:344–352.

Becker JA, Hedden T, Carmasin J, Maye J, Rentz DM, Putcha D, et al. (2011): Amyloid-beta associated cortical thinning in clinically normal elderly. Ann Neurol 69:1032–1042.

Bennett DA, Schneider JA, Arvanitakis Z, Kelly JF, Aggarwal NT, Shah RC, et al. (2006): Neuropathology of older persons without cognitive impairment from two community-based studies. Neurology 66:1837–1844.

Benton AL, Hamsher K, Sivan AB (1983): Multilingual Aphasia Examination. Iowa City, IA: AJA Associates.

Bero AW, Yan P, Roh JH, Cirrito JR, Stewart FR, Raichle ME, et al. (2011): Neuronal activity regulates the regional vulnerability to amyloid-beta deposition. Nat Neurosci 14:750–756.

Bourgeat P, Chetelat G, Villemagne VL, Fripp J, Raniga P, Pike K, et al. (2010): Beta-amyloid burden in the temporal neocortex is related to hippocampal atrophy in elderly subjects without dementia. Neurology 74:121–127.

Braak H, Braak E (1991): Demonstration of amyloid deposits and neurofibrillary changes in whole brain sections. Brain Pathol 1:213–216.

Buckner RL, Snyder AZ, Shannon BJ, LaRossa G, Sachs R, Fotenos AF, et al. (2005): Molecular, structural, and functional characterization of Alzheimer's disease: Evidence for a relationship between default activity, amyloid, and memory. J Neurosci 25:7709–7717.

Buckner RL, Sepulcre J, Talukdar T, Krienen FM, Liu H, Hedden T, et al. (2009): Cortical hubs revealed by intrinsic functional connectivity: Mapping, assessment of stability, and relation to Alzheimer's disease. J Neurosci 29:1860–1873.

Busche MA, Eichhoff G, Adelsberger H, Abramowski D, Wiederhold KH, Haass C, et al. (2008): Clusters of hyperactive neurons near amyloid plaques in a mouse model of Alzheimer's disease. Science 321:1686–1689.

Caselli RJ, Reiman EM, Osborne D, Hentz JG, Baxter LC, Hernandez JL, et al. (2004): Longitudinal changes in cognition and behavior in asymptomatic carriers of the APOE e4 allele. Neurology 62:1990–1995.

Chetelat G, Desgranges B, Landeau B, Mezenge F, Poline JB, de la Sayette V, et al. (2008): Direct voxel-based comparison between grey matter hypometabolism and atrophy in Alzheimer's disease. Brain 131 (Part 1):60–71.

Cirrito JR, Yamada KA, Finn MB, Sloviter RS, Bales KR, May PC, et al. (2005): Synaptic activity regulates interstitial fluid amyloid-beta levels in vivo. Neuron 48:913–922.

Cohen AD, Price JC, Weissfeld LA, James J, Rosario BL, Bi W, et al. (2009): Basal cerebral metabolism may modulate the cognitive effects of Abeta in mild cognitive impairment: An example of brain reserve. J Neurosci 29:14770–14778.

Dale AM, Fischl B, Sereno MI (1999): Cortical surface-based analysis. I. Segmentation and surface reconstruction. Neuroimage 9:179–194.

Delis DC, Kramer JH, Kaplan E, Ober BA (2000): California Verbal Learning Test, 2nd ed. San Antonio, TX: Psychological Corporation.

Desikan RS, Segonne F, Fischl B, Quinn BT, Dickerson BC, Blacker D, et al. (2006): An automated labeling system for subdividing the human cerebral cortex on MRI scans into gyral based regions of interest. Neuroimage 31:968–980.

Dickerson BC, Salat DH, Greve DN, Chua EF, Rand-Giovannetti E, Rentz DM, et al. (2005): Increased hippocampal activation in mild cognitive impairment compared to normal aging and AD. Neurology 65:404–411.

Dickerson BC, Bakkour A, Salat DH, Feczko E, Pacheco J, Greve DN, et al. (2009): The cortical signature of Alzheimer's disease: Regionally specific cortical thinning relates to symptom severity in very mild to mild AD dementia and is detectable in asymptomatic amyloid-positive individuals. Cereb Cortex 19:497–510.

Drzezga A, Becker JA, Van Dijk KR, Sreenivasan A, Talukdar T, Sullivan C, et al. (2011): Neuronal dysfunction and disconnection of cortical hubs in non-demented subjects with elevated amyloid burden. Brain 134 (Part 6):1635–1646.

Edison P, Archer HA, Hinz R, Hammers A, Pavese N, Tai YF, et al. (2007): Amyloid, hypometabolism, and cognition in Alzheimer disease: An [11C]PIB and [18F]FDG PET study. Neurology 68:501–508.

Fellin T, Pascual O, Gobbo S, Pozzan T, Haydon PG, Carmignoto G (2004): Neuronal synchrony mediated by astrocytic glutamate through activation of extrasynaptic NMDA receptors. Neuron 43:729–743.

Fischl B, Liu A, Dale AM (2001): Automated manifold surgery: Constructing geometrically accurate and topologically correct models of the human cerebral cortex. IEEE Trans Med Imaging 20:70–80.

Fischl B, Salat DH, Busa E, Albert M, Dieterich M, Haselgrove C, et al. (2002): Whole brain segmentation: Automated labeling of neuroanatomical structures in the human brain. Neuron 33:341–355.

Golden CJ (1978): Stroop Color and Word Test: A Manual for Clinical and Experimental Uses. Chicago: Stoelting.

Good CD, Johnsrude IS, Ashburner J, Henson RN, Friston KJ, Frackowiak RS (2001): A voxel-based morphometric study of ageing in 465 normal adult human brains. Neuroimage, 14 (1 Part 1):21–36.

Habeck C, Stern Y (2010): Multivariate data analysis for neuroimaging data: Overview and application to Alzheimer's disease. Cell Biochem Biophys 58:53–67.

Habeck C, Krakauer JW, Ghez C, Sackeim HA, Eidelberg D, Stern Y, et al. (2005): A new approach to spatial covariance modeling of functional brain imaging data: Ordinal trend analysis. Neural Comput 17:1602–1645.

Habeck C, Foster NL, Perneczky R, Kurz A, Alexopoulos P, Koeppe RA, et al. (2008): Multivariate and univariate neuroimaging biomarkers of Alzheimer's disease. Neuroimage 40:1503–1515.

Hardy J, Selkoe DJ (2002): The amyloid hypothesis of Alzheimer's disease: Progress and problems on the road to therapeutics. Science 297:353–356.

Itagaki S, McGeer PL, Akiyama H, Zhu S, Selkoe D (1989): Relationship of microglia and astrocytes to amyloid deposits of Alzheimer disease. J Neuroimmunol 24:173–182.

Jack CR Jr, Lowe VJ, Senjem ML, Weigand SD, Kemp BJ, Shiung MM, et al. (2008): 11C PiB and structural MRI provide complementary information in imaging of Alzheimer's disease and amnestic mild cognitive impairment. Brain 131: 665–680.

Jack CR Jr, Lowe VJ, Weigand SD, Wiste HJ, Senjem ML, Knopman DS, et al. (2009): Serial PIB and MRI in normal, mild cognitive impairment and Alzheimer's disease: Implications for sequence of pathological events in Alzheimer's disease. Brain 132:1355–1365.

Jack CR Jr, Knopman DS, Jagust WJ, Shaw LM, Aisen PS, Weiner MW, et al. (2010): Hypothetical model of dynamic biomarkers of the Alzheimer's pathological cascade. Lancet Neurol 9:119–128.

Jagust WJ, Mormino EC. (2011): Lifespan brain activity, beta-amyloid, and Alzheimer's disease. Trends Cogn Sci 15:520–526.

Kadir A, Almkvist O, Forsberg A, Wall A, Engler H, Langstrom B, et al. (2012): Dynamic changes in PET amyloid and FDG imaging at different stages of Alzheimer's disease. Neurobiol Aging 33:198.e1–198.e14.

Kamenetz F, Tomita T, Hsieh H, Seabrook G, Borchelt D, Iwatsubo T, et al. (2003): APP processing and synaptic function. Neuron 37:925–937.

Kang JE, Lim MM, Bateman RJ, Lee JJ, Smyth LP, Cirrito JR, et al. (2009): Amyloid-beta dynamics are regulated by orexin and the sleep-wake cycle. Science 326:1005–1007.

Klunk WE, Engler H, Nordberg A, Wang Y, Blomqvist G, Holt DP, et al. (2004): Imaging brain amyloid in Alzheimer's disease with Pittsburgh Compound-B. Ann Neurol 55:306–319.

Logan J, Fowler JS, Volkow ND, Wang GJ, Ding YS, Alexoff DL (1996): Distribution volume ratios without blood sampling from graphical analysis of PET data. J Cereb Blood Flow Metab 16:834–840.

Mathis CA, Wang Y, Holt DP, Huang GF, Debnath ML, Klunk WE (2003): Synthesis and evaluation of 11C-labeled 6-substituted 2-arylbenzothiazoles as amyloid imaging agents. J Med Chem 46:2740–2754.

Minoshima S, Giordani B, Berent S, Frey KA, Foster NL, Kuhl DE (1997): Metabolic reduction in the posterior cingulate cortex in very early Alzheimer's disease. Ann Neurol 42:85–94.

Moeller JR, Strother SC, Sidtis JJ, Rottenberg DA (1987): Scaled subprofile model: A statistical approach to the analysis of functional patterns in positron emission tomographic data. J Cereb Blood Flow Metab 7:649–658.

Mormino EC, Kluth JT, Madison CM, Rabinovici GD, Baker SL, Miller BL, et al. (2009): Episodic memory loss is related to hippocampal-mediated beta-amyloid deposition in elderly subjects. Brain 132:1310–1323.

Mormino EC, Brandel MG, Madison CM, Marks S, Baker SL, Jagust WJ (2011): Aβ Deposition in Aging is Associated with Increases in Brain Activation during Successful Memory Encoding. Cereb Cortex. Epub ahead of print.

Oh H, Mormino EC, Madison C, Hayenga A, Smiljic A, Jagust WJ (2011): Beta-Amyloid affects frontal and posterior brain networks in normal aging. Neuroimage 54:1887–1895.

Oh H, Madison C, Haight TJ, Markley C, Jagust WJ (2012): Effects of age and beta-amyloid on cognitive changes in normal elderly people. Neurobiol Aging. Epub ahead of print.

Palop JJ, Mucke L (2009): Epilepsy and cognitive impairments in Alzheimer disease. Arch Neurol 66:435–440.

Palop JJ, Mucke L (2010): Amyloid-beta-induced neuronal dysfunction in Alzheimer's disease: From synapses toward neural networks. Nat Neurosci 13:812–818.

Pike KE, Savage G, Villemagne VL, Ng S, Moss SA, Maruff P, et al. (2007): Beta-amyloid imaging and memory in non-demented individuals: Evidence for preclinical Alzheimer's disease. Brain 130:2837–2844.

Price JC, Klunk WE, Lopresti BJ, Lu X, Hoge JA, Ziolko SK, et al. (2005): Kinetic modeling of amyloid binding in humans using PET imaging and Pittsburgh Compound-B. J Cereb Blood Flow Metab 25:1528–1547.

Puzzo D, Privitera L, Leznik E, Fa M, Staniszewski A, Palmeri A, et al. (2008): Picomolar amyloid-beta positively modulates synaptic plasticity and memory in hippocampus. J Neurosci 28:14537–14545.

Reiman EM, Chen K, Alexander GE, Caselli RJ, Bandy D, Osborne D, et al. (2004): Functional brain abnormalities in young adults at genetic risk for late-onset Alzheimer's dementia. Proc Natl Acad Sci USA 101:284–289.

Reitan RM (1958): Validity of the Trail Making Test as an indicator of organic brain damage. Percept Motor Skills 8:271–276.

Segonne F, Dale AM, Busa E, Glessner M, Salat D, Hahn HK, et al. (2004): A hybrid approach to the skull stripping problem in MRI. Neuroimage 22:1060–1075.

Selkoe DJ (2001): Alzheimer's disease: Genes, proteins, and therapy. Physiol Rev 81:741–766.

Silverman DH, Small GW, Chang CY, Lu CS, Kung De Aburto MA, Chen W, et al. (2001): Positron emission tomography in evaluation of dementia: Regional brain metabolism and long-term outcome. JAMA 286:2120–2127.

Smith A (1982): Symbol Digits Modalities Test. Los Angeles, CA: Western Psychological Services.

Sorg C, Riedl V, Muhlau M, Calhoun VD, Eichele T, Laer L, et al. (2007): Selective changes of resting-state networks in individuals at risk for Alzheimer's disease. Proc Natl Acad Sci USA 104:18760–18765.

Sperling RA, Laviolette PS, O'Keefe K, O'Brien J, Rentz DM, Pihlajamaki M, et al. (2009): Amyloid deposition is associated with impaired default network function in older persons without dementia. Neuron 63:178–188.

Tosun D, Schuff N, Mathis CA, Jagust W, Weiner MW (2011): Spatial patterns of brain amyloid-beta burden and atrophy rate associations in mild cognitive impairment. Brain 134 (Part 4):1077–1088.

Vaishnavi SN, Vlassenko AG, Rundle MM, Snyder AZ, Mintun MA, Raichle ME (2010): Regional aerobic glycolysis in the human brain. Proc Natl Acad Sci USA 107:17757–17762.

Vezzani A, Granata T (2005): Brain inflammation in epilepsy: Experimental and clinical evidence. Epilepsia 46:1724–1743.

Villemagne VL, Pike KE, Darby D, Maruff P, Savage G, Ng S, et al. (2008): Abeta deposits in older non-demented individuals with cognitive decline are indicative of preclinical Alzheimer's disease. Neuropsychologia 46:1688–1697.

Vlassenko AG, Vaishnavi SN, Couture L, Sacco D, Shannon BJ, Mach RH, et al. (2010): Spatial correlation between brain aerobic glycolysis and amyloid-beta (Abeta) deposition. Proc Natl Acad Sci USA 107:17763–17767.

Wechsler D (1997): Wechsler Adult Intelligence Scale-III (WAIS-III) Manual. New York: The Psychological Corporation.

Yan P, Bero AW, Cirrito JR, Xiao Q, Hu X, Wang Y, et al. (2009): Characterizing the appearance and growth of amyloid plaques in APP/PS1 mice. J Neurosci 29:10706–10714.